AGU PUBLICATIONS

Geophysical Research Letters

RESEARCH LETTER

10.1002/2013GL058650

Key Points:
- Wave height increases are projected for the tropics and for SH high latitudes
- The frequency of a fixed-size extreme wave height could double or triple
- The projections show increased wave heights accompanied by increased variability

Supporting Information:
- Readme
- Supplementary Figures and Table

Correspondence to:
X. L. Wang,
Xiaolan.Wang@ec.gc.ca

Citation:
Wang, X. L., Y. Feng, and V. R. Swail (2014), Changes in global ocean wave heights as projected using multimodel CMIP5 simulations, *Geophys. Res. Lett.*, *41*, 1026–1034, doi:10.1002/2013GL058650.

Received 11 NOV 2013
Accepted 2 JAN 2014
Accepted article online 7 JAN 2014
Published online 15 FEB 2014

Changes in global ocean wave heights as projected using multimodel CMIP5 simulations

Xiaolan L. Wang[1], Yang Feng[1], and Val R. Swail[1]

[1]Climate Research Division, Science and Technology Branch, Environment Canada, Toronto, Ontario, Canada

Abstract Ocean surface waves can be major hazards in coastal and offshore activities. However, there exists very limited information on ocean wave behavior in response to climate change, because such information is not simulated in current global climate models. This study made statistical projections of changes in ocean wave heights using sea level pressure (SLP) information from 20 CMIP5 (Coupled Model Intercomparison Project Phase 5) global climate models for the 21st century. The results show significant wave height increases in the tropics (especially in the eastern tropical Pacific) and in Southern Hemisphere high latitudes (south of 45°S). Under the projected 2070–2099 climate condition of the rising high concentration pathway—the RCP8.5 scenario, the occurrence frequency of the present-day one in 10 year extreme wave heights is likely to double or triple in several coastal regions around the world. These wave height increases are primarily driven by increased SLP gradients and hence increased surface wind energy.

1. Introduction

Ocean surface waves are generated by surface winds locally (wind-sea) and/or remotely (swell). Ocean waves can be major hazards in coastal and offshore operations and activities. For example, they contribute significantly to coastal sea level extremes and subsequent flooding. Also, waves are a key factor affecting coastal erosion and sediment budgets. Waves play an important role in the climate system; they are involved in several key processes at the air-sea interface, such as momentum fluxes, energy and heat fluxes, mass fluxes, and radiation budget [*Hemer et al.*, 2012]. As an important climate element, ocean waves are likely to be affected by anthropogenic forcing. There is increasing evidence for changes in ocean waves over past decades [e.g., *Young et al.*, 2011, 2012]. Such changes have been found to be attributable to external forcing (including natural and anthropogenic forcing) [*Wang et al.*, 2008].

While information on wave climate change is of critical importance for almost all aspects of coastal and offshore activities, it is very limited, as acknowledged recently at the first workshop of the Coordinated Ocean Wave Climate Projections project [*Hemer et al.*, 2012]. Since ocean waves information is not simulated in current global climate models, dynamical and/or statistical modelling methods have been used to obtain information on wave climate changes. Dynamical modelling of ocean waves uses climate model simulated surface winds to drive a numerical wave model [*Mori et al.*, 2010; *Hemer et al.*, 2013a, 2013b]. It is highly computationally demanding and depends heavily on the quality of the surface winds simulated by climate models, and surface winds are usually not as well represented in climate models as the mean sea level pressure (SLP) fields [*Wang et al.*, 2009]. Thus, dynamical wave projections have been conducted only in time-slice experiments for projections by a single climate model [*Mori et al.*, 2010] or a few climate models [*Hemer et al.*, 2013a, 2013b]. Statistical modelling approaches are typically based on an empirical relationship between a wave variable, such as significant wave height, and atmospheric variables, such as the SLP and the squared SLP (spatial) gradients [e.g., *Wang and Swail*, 2006a, 2006b; *Wang et al.*, 2012], assuming that the relationship holds under the future climate conditions. It requires much less computational power than dynamical modelling. Thus, statistical wave simulations can be conducted for large numbers of climate simulations, and for multimodel ensembles, such as the multimodel historical and future scenarios simulations of the Coupled Model Intercomparison Project Phase 5 (CMIP5) [*Taylor et al.*, 2012].

Analyzing a seven-model ensemble of CMIP3-based projections for a set of SRES emissions (A1b, A2, B2, and IS92a) [*Nakicenovic and Swart*, 2000], *Hemer et al.* [2013a] reported on projected changes in annual/seasonal mean significant wave heights (H_s), mean wave period, and mean wave direction. However, they did not assess changes in extreme wave heights. This is primarily because subdaily SLP fields were not available from the CMIP3 archive, and 14 of the 20 ensemble members they analyzed are statistical projections of

seasonal mean and maximum H_s based on monthly mean SLP fields simulated by three CMIP3 climate models for three scenarios [*Wang and Swail*, 2006a].

The CMIP5 climate models are generally of higher spatial resolution compared with the CMIP3 models, and 6-hourly data are available for a large number of the CMIP5 climate models (see next section for details). We used 6-hourly SLP data from 20 CMIP5 models simulations to make statistical projections of 6-hourly H_s and derived annual/seasonal extreme wave heights to assess projected changes in extreme wave heights. Further, we took an extreme value probability analysis approach to estimate changes in the recurrence/waiting time (frequency) of extreme wave heights, which is more directly related to the impacts of wave heights on coastal/marine infrastructure design and risk management than is the annual mean and annual maximum H_s.

2. Model and Data

We used a statistical model recently developed by *Wang et al.* [2012] to project changes in significant wave heights (H_s) in the global oceans that correspond to changes in the SLP fields from the CMIP5 simulations for two Representative Concentration Pathways (RCPs; i.e., emissions scenarios): RCP4.5 and RCP8.5 [*Moss et al.*, 2008]. This statistical modeling approach is detailed in *Wang et al.* [2012] and also summarized in the supporting information section S1. We used the 6-hourly H_s and SLP data from the ERA-Interim Reanalysis [*Dee et al.*, 2011] to calibrate and evaluate the statistical wave model. The evaluation results are presented and briefly discussed in the supporting information section S2.

The focus of this study is on the global scale. We divided the oceans into 11 regions, as detailed in the supporting information Table S1 and Figure S2, and let each region have its own set of leading principal components of the corresponding SLP and SLP gradient fields, which account for some regional differences. Nevertheless, the skill of the statistical model can be improved for enclosed or semienclosed basins or coastal zones (such as the South China Sea or the Caribbean Sea) by modeling each of such areas individually, using a smaller SLP field that is more representative of the wave height variability in the area. This is the focus of our ongoing regional studies.

In general, the model has slightly higher skills in the tropics and in the high latitudes than in the midlatitudes of each hemisphere in all seasons (supporting information Figure S3). Therefore, higher confidence can be placed on the resulting H_s for the high latitudes and the tropics. Nevertheless, the statistical modeling of H_s reproduced well the climate for both annual mean H_s and annual maximum H_s (Figure 1) as represented in the dynamical wave reanalyses of both the ERA40 [*Uppala et al.*, 2005; *Caires et al.*, 2004a, 2004b] and the ERA-Interim [*Dee et al.*, 2011]. It is particularly interesting to note that our statistical simulations of 6-hourly H_s well reproduced the climate of annual maximum H_s, with only slight underestimation in the tropics and some overestimation in the region off the North America east coast (Figures 1a–1c). Note that the ERA-Interim wave data were used to calibrate the statistical wave model, but the ERA40 wave data were not.

We focused on CMIP5 simulations from the 20 global climate models listed in Table 1. These models were selected because 6-hourly SLP data for historical, RCP4.5, and RCP8.5 simulations [*Taylor et al.*, 2012] were available when this study was initiated and their spatial resolution is reasonable to resolve key wave features (see Table 1). We used only one simulation (the first run) from each climate model, considering the fact that some climate models had only one simulation available (Table 1).

The RCP4.5 scenario is an intermediate "stabilization without overshoot" pathway in which radiative forcing is stabilized at approximately 4.5 W/m^2 after 2100. The RCP8.5 scenario is a high pathway for which radiative forcing reaches $>$ 8.5 W/m^2 by 2100 and continues to rise for some amount of time [*Moss et al.*, 2008]. As clarified in *Moss et al.* [2008], "RCPs are representative of plausible alternative scenarios for the future but are not predictions or forecasts of future outcomes. No RCP is intended as a 'best guess,' most likely, or most plausible projection."

The CMIP5 SLP data had different spatial resolutions (Table 1) and were converted to a common 2°-by-2° latitude-longitude grid (about the midrange of resolution for the 20 models). The ERA-Interim SLP data used in this study are on the same 2°-by-2° grid, and the ERA-Interim H_s data, on a 1°-by-1° latitude-longitude

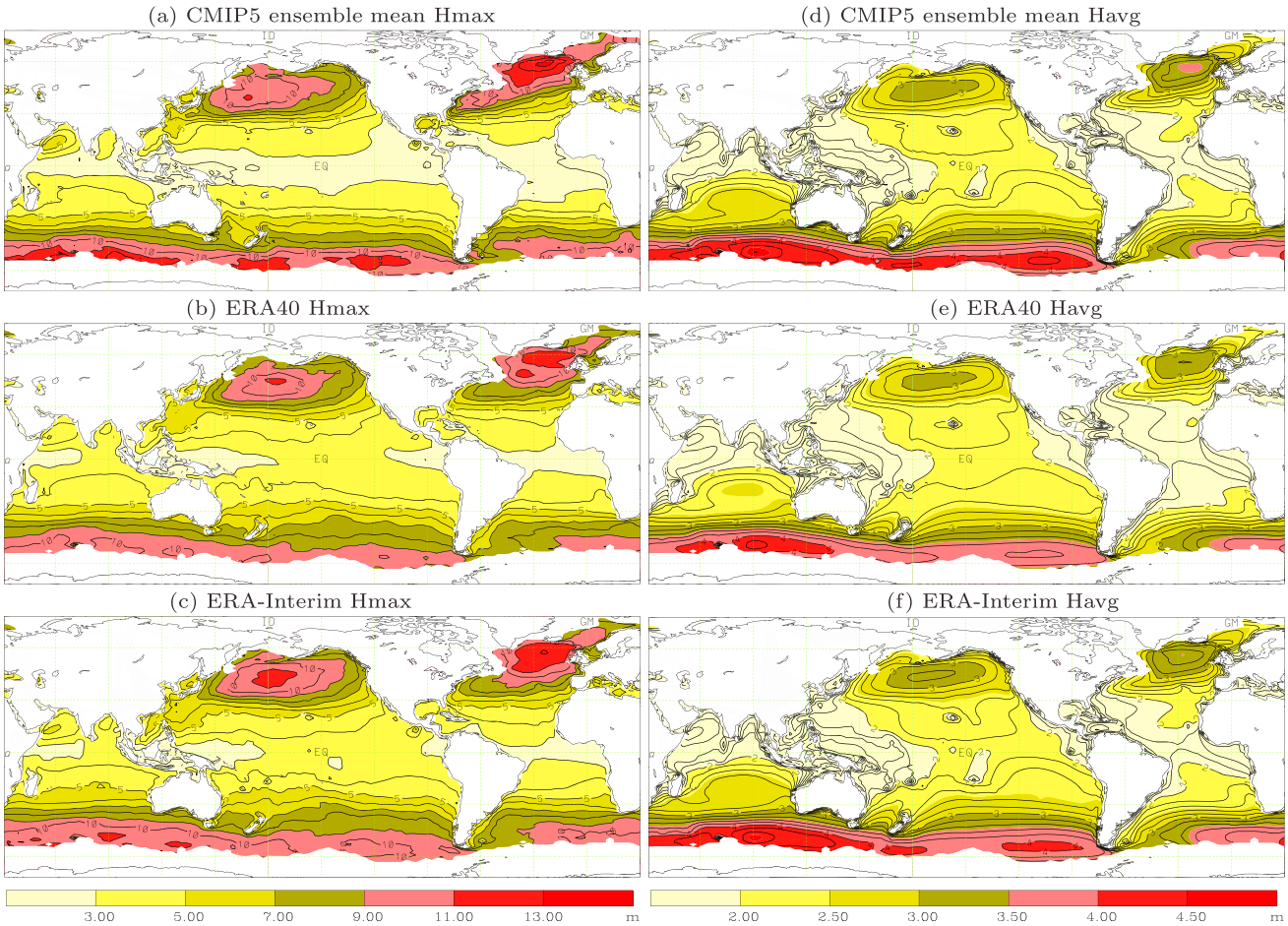

Figure 1. (a–f) The 1980–1999 climatological fields of annual mean and annual maximum significant wave heights (Havg and Hmax; in meters) as derived from the ensemble mean of CMIP5-based historical simulations and from the ERA40 and ERA-Interim wave reanalyses.

grid. All the SLP and H_s data are 6-hourly instantaneous values (i.e., as output from the corresponding model for the specific time step).

In order to diminish climate model biases, the model SLP simulations were adjusted such that they have the same climatological mean and standard deviation as the ERA-Interim SLP data (used as proxy for observations) over the period 1981–2000. For each climate model, only the first run (run 1) of the historical simulations is used to estimate the simulated climatological mean and standard deviation for the period 1981–2000. Such adjustments are also necessary for applying the Box-Cox transformations [*Box and Cox*, 1964] that were optimized for the ERA-Interim squared SLP gradients to the simulated squared SLP gradients (see also supporting information section S1). A brief discussion on the climate models fidelity is provided in the supporting information section S3.

Time series of SLP-based predictors were derived from each CMIP5 run and were fed into the calibrated statistical wave model to predict 6-hourly H_s for the 150 year period from 1950 to 2099. From the resulting 6-hourly H_s, time series of annual/seasonal mean and maximum H_s were derived and used to assess wave height climate changes.

A one in 10 year extreme is an extreme value that is expected to be exceeded, on average, once every 10 years, i.e., an extreme of a recurrence time (also called waiting time) of 10 years. In order to assess changes in the recurrence time of one in 10 year extreme H_s, we fit a Generalized Extreme Value (GEV) distribution to the projected annual maximum H_s for the period 1970–1999 (present) and for the period 2070–2099 (future), subsequently. We used the GEV distribution for the present period to estimate one in 10 year extreme H_s under the present climate condition (i.e., present-day one in 10 year extreme) and used the GEV

Table 1. The 20 Global Climate Models of CMIP5 Simulations Analyzed in This Study and Their Resolutions, and Numbers of Historical, RCP4.5, and RCP8.5 Runs Available at Time of our Downloading of the Data[a]

Model Name	Resolution Latitude × Longitude L#(T#)	Runs	Institution
ACCESS1.0	145 × 192 L38	1,1,1	Commonwealth Scientific and Industrial Research Organization (CSIRO) and Bureau of Meteorology, Australian
BCC-CSM1-1	64 × 128 L26(T42)	3,1,1	Beijing Climate Center, China Meteorological Administration
BCC-CSM1-1(m)	160 × 320 L26(T106)	3,1,1	Beijing Climate Center, China Meteorological Administration
CanESM2	64 × 128 L35(T63)	5,1,1	Canadian Centre for Climate Modelling and Analysis
CCSM4	192 × 288 L27	1,1,1	National Center for Atmospheric Research, USA
CNRM-CM5	128 × 256 L31(T127)	10,1,1	Centre National de Recherches Meteorologiques, Meteo-France
CSIRO-Mk3-6-0	96 × 192 L18(T63)	10,10, 10	Australian Commonwealth Scientific and Industrial Research Organization
EC-EARTH	160 × 320 L62(T159)	7,1,2	Royal Netherlands Meteorological Institute
FGOALS-s2	128 × 108 L26	3,3,3	Instute of Atmospheric Physics, Chinese Academy of Sciences
GFDL-ESM2M	90 × 144 L24	1,1,1	Geophysical Fluid Dynamics Laboratory, USA
HadGEM2-ES	145 × 192 L40	1,1,1	UK Met Office Hadley Centre
INMCM4	120 × 180 L21	1,1,1	Institute for Numerical Mathematics, Russia
IPSL-CM5A-MR	143 × 144 L39	2,1,1	Institut Pierre-Simon Laplace, France
MIROC5	128 × 256 L40(T85)	4,3,3	Model for Interdisciplinary Research on Climate, Japan
MIROC-ESM	64 × 128 L80(T42)	3,1,1	Model for Interdisciplinary Research on Climate, Japan
MIROC-ESM-CHEM	64 × 128 L80(T42)	1,1,1	Model for Interdisciplinary Research on Climate, Japan
MPI-ESM-LR	96 × 192 L47(T63)	3,3,3	Max Planck Institute for Meteorology, Germany
MPI-ESM-MR	96 × 192 L95(T63)	3,3,1	Max Planck Institute for Meteorology, Germany
MRI-CGCM3	160 × 320 L48(TL159)	5,1,1	Meteorological Research Institute, Japan
NorESM1-M	96 × 144 L26	3,1,1	Norwegian Climate Centre

[a]Model resolution is represented by the size of a horizontal grid (Latitude × Longitude) on which model output is available and by the number of vertical levels (L#). Spectral models are also characterized by their spectral truncations (T#).

distribution for the future period to estimate the recurrence time of the present-day one in 10 year extreme under the projected future climate conditions. This was done for each of the 20 models' projections. The 20-model ensemble mean recurrence time was then estimated as the inverse of the ensemble mean recurrence frequency of the present-day one in 10 year extreme under the projected future climate condition. Our choice of using the GEV approach with 30 years of data to estimate one in 10 year extremes is based on the finding of *Wang et al.* [2013] who reported that different approaches for estimating extremes have comparable estimation stability when the sample size is more than twice the waiting time of the extreme to be estimated (here the sample size is 3 times the waiting time).

Note that extreme H_s conditions, especially those associated with tropical cyclones, are likely underestimated due to the relatively course resolutions of the 20 global climate models, although the extreme conditions as represented in the ERA-Interim and ERA40 reanalyses were reasonably well reproduced (with only slight underestimation in the tropics; see Figures 1a–1c). In this case, it makes more sense to estimate changes in extreme H_s than to estimate the actual values of extreme H_s per se. Thus, the focus of this study is on estimation of H_s changes projected for the late 21st century.

3. Projected Wave Height Changes

For the RCP8.5 scenario, Figure 2 shows the 20-model ensemble mean projected changes in annual/seasonal mean and maximum H_s for the period 2080–2099 relative to the period 1980–1999 (i.e., the difference between the climates of the two 20 year periods). The ensemble mean here is a simple arithmetic mean, because there are no notable differences between this simple arithmetic mean and the inverse-error weighted ensemble mean (see supporting information section S3). We used the intermodel standard

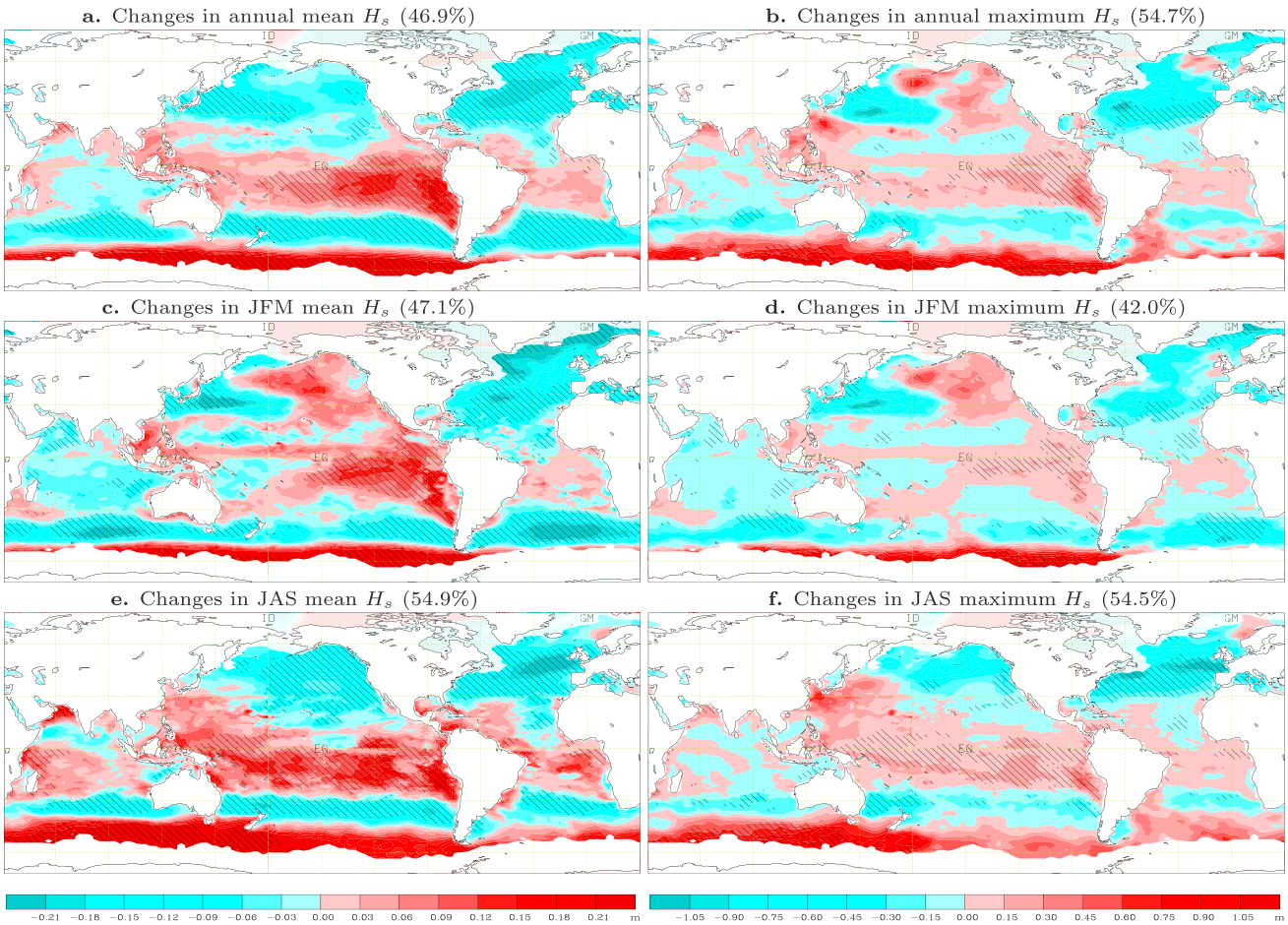

Figure 2. (a–f) The 20-model ensemble mean of projected changes in annual/seasonal mean and maximum significant wave heights (H_s, m) for the period 2080–2099 relative to the period 1980–1999 for the RCP8.5 scenario. Hatchings indicate areas where the multimodel ensemble mean exceeds the intermodel standard deviation. The percentage of area with projected H_s increases are shown in parentheses on top of each panel.

deviation as a measure of "model uncertainty," namely, the uncertainty due to the use of different climate models (also referred to as intermodel variability).

For the annual mean and maximum H_s, the ensemble mean projected increases are seen in about 50% of the global ocean area (Figures 2a–2b); at about 50% of these locations the projected increases are within the range of 0.05 to 0.31 m (0.02 to 0.10 m) for annual maximum (mean) H_s. The global maximum increase (in the ensemble mean projection) is 1.88 m for annual maximum H_s, and 0.42 m for annual mean H_s; both are seen in the SH high latitudes, at grid points (56°S, 113°E) and (59°S, 171°E), respectively.

For both annual mean and maximum H_s, the changes between the two 20 year periods are characterized by increases in the eastern tropical Pacific and Southern Hemisphere (SH) high latitudes, with decreases in the SH midlatitudes and the midlatitudes of the North Atlantic (Figure 2). These changes are reasonably robust among the 20 climate models, because the ensemble mean changes are greater than one intermodel standard deviation (hatched areas in Figure 2). However, the 20 climate models appear to have better agreement in projecting changes in the annual means than in the annual maxima (the hatched areas are more extensive in Figure 2 (left) than in the corresponding Figure 2 (right)). This is at least in part due to the resolution differences among the climate models (Table 1). At this range of model resolution, higher resolution models generally represent extremes better than lower resolution models, while all these models have a resolution that can represent the mean states about equally well. Despite of our conversion of the model data to a common 2°-by-2° grid, the effect of climate model resolution on extreme wave heights is still discernible. The individual climate model projections of change in annual maximum H_s are shown in the supporting information Figure S6. The EC-EARTH and MRI-CGCM3, which are of the highest spatial resolution among

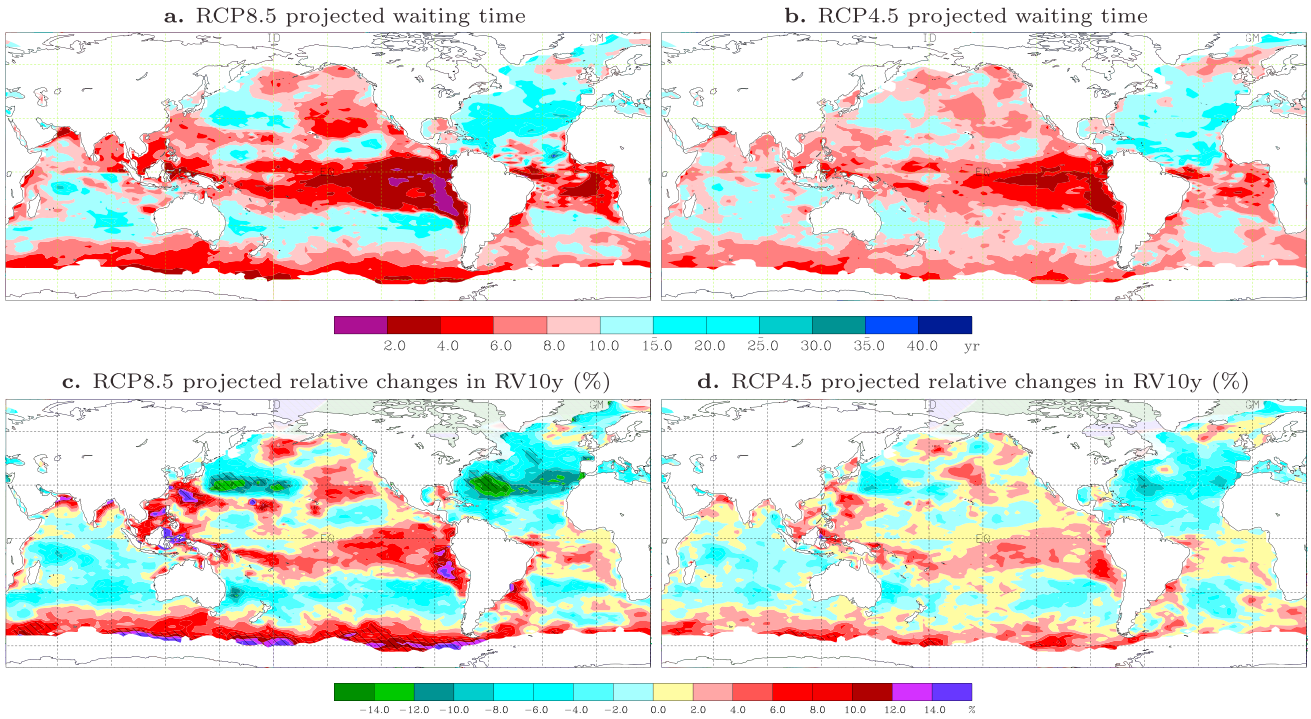

Figure 3. (a and b) The 20-model ensemble mean of projected waiting time of the present-day (1970–1999) one in 10 year extreme H_s for the period 2070–2099, for RCP8.5 and RCP4.5 scenarios. The unit is year. (c and d) The 20-model ensemble mean projected changes in the one in 10 year extreme H_s (RV10y) for the period 2070–2099, expressed in percentage of the present-day one in 10 year extreme H_s. Hatchings indicate areas where the multimodel ensemble mean exceeds the intermodel standard deviation.

the 20 models (Table 1), projected wave height increases in much more extensive areas (Figure S6) than the other models. The two Max-Planck-Institut models also projected more extensive increases in wave heights (Figure S6) although they are of moderate resolution (Table 1).

The projected wave height changes also show notable seasonality that varies by region. In particular, the eastern North Pacific is projected to have increases in winter (JFM for January–March) but decreases in summer (JAS for July–September) (Figures 2c–2f). The western North Pacific, the western tropical Pacific, and the tropical Indian Ocean are projected to have decreases in JFM but increases in JAS (Figures 2c–2f). For the high-latitude North Pacific, changes in the annual maximum wave height are dominated by changes in the winter maximum wave height (Figure 2, right), but changes in the annual mean wave height are dominated by changes in the summer mean wave heights (Figure 2, left). This indicates that the extreme wave heights in this region primarily occur in winter, as would be expected.

The occurrence frequency of the present-day one in 10 year extreme wave heights is likely to double or triple in several coastal regions around the world under the projected 2070–2099 climate of the RCP8.5 scenario. For both RCP8.5 and RCP4.5 scenarios, Figure 3 shows the 20-model ensemble mean projected waiting time of the present-day (1970–1999) one in 10 year extremes of H_s for the period 2070–2099 (Figures 3a–3b), and the 20-model ensemble mean projected relative changes in the one in 10 year extreme H_s for the period 2070–2099 (Figures 3c–3d). The relative changes are expressed in percentage of the present-day one in 10 year extreme H_s. Under the projected 2070–2099 climate condition of the RCP8.5 scenario, the present-day one in 10 year extreme wave heights are expected to be exceeded on average once every 1–4 years along the Chilean and Columbia's coasts, once every 4–6 years in the Gulf of Oman and along the Mexican Baja coast, along the Vietnamese coast, and along the west Tasmanian coast, and once every 6–8 years along the Danish coast and the Canadian west coast, and in the Gulf of Mexico (Figure 3a). As shown in Figure 3b, the changes associated with RCP4.5 have a similar pattern but are weaker than those associated with RCP8.5. In terms of the relative changes for the period 2070–2099, the one in 10 year extreme wave heights along the Chilean and Columbia's coasts are projected to increase by 10–15% for the RCP8.5 scenario (Figure 3c), by 7–10% for the RCP4.5 scenario (Figure 3d).

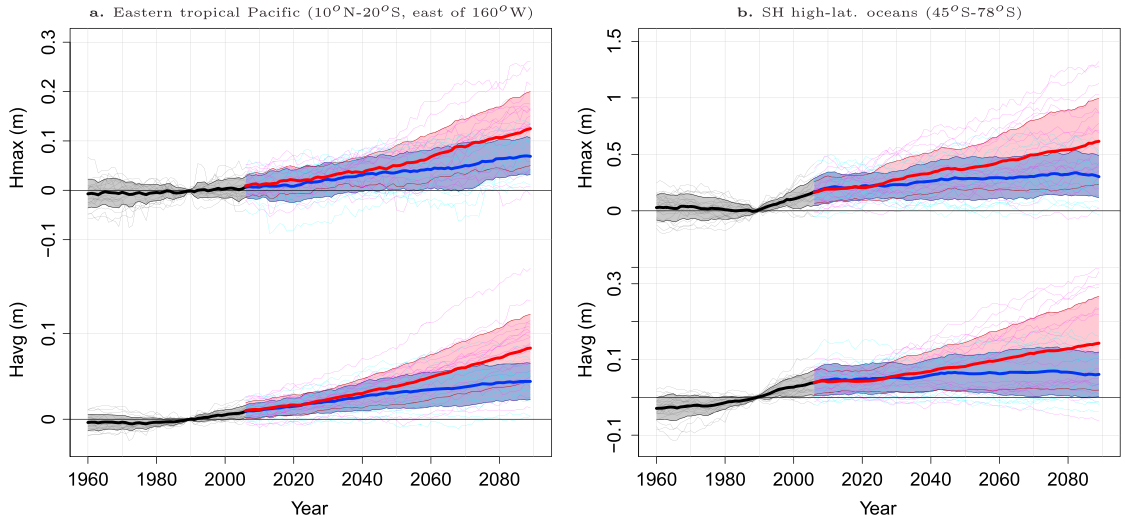

Figure 4. (a–b) Projected changes in the regional-averaged annual means (Havg) and annual maxima (Hmax) of significant wave heights, relative to the 1980–1999 climate of the corresponding statistic (Havg or Hmax), for the eastern tropical Pacific and the SH high-latitude oceans. The regional averages are grid cell area weighted. Each time series is a 21 year moving average series of the projected changes. The thick lines show the 20-model ensemble mean changes in the historical (black), the RCP4.5 (blue), and the RCP8.5 (red) simulations. Each thin line shows the changes projected by one climate model individually. The shadings indicate one intermodel standard deviation below and above the respective ensemble mean.

Further, our supplementary analysis (see supporting information section S4 and Figure S7) reveals that the regions of projected wave height increases (decreases) are also projected to have increases (decreases) in the wave height variability and that the increases in wave height variability are mainly in the intraannual variability. However, the variability changes are less outstanding against the intermodel variability than are the wave height changes, especially in the eastern tropical Pacific. Changes in the high-latitude North Pacific wave height variability are dominated by changes in winter, with the changes in the all-season variability resembling the changes in the JFM variability (Figure S7).

4. Intermodel and Interscenario Variability

To illustrate the intermodel and interscenario variability, Figure 4 shows the projected changes in the regional-averaged annual mean and maximum H_s for the eastern tropical Pacific and SH high latitudes. Here the regional averages are grid cell area weighted; each time series is a 21 year moving average series of the projected wave height changes. For both scenarios, almost all the 20 models project wave height increases by the end of the 21st century in these regions (Figure 4). For the SH high latitudes, the ensemble mean changes in the annual maximum wave height stand out more clearly from the intermodel variability than those in the annual mean wave height (Figure 4b).

For the global average (not shown), the 20-model ensemble mean shows a slight increase in the annual maximum wave height, which, however, does not stand out of the intermodel variability; while it does not show any significant change in annual mean wave heights. This is true for both RCP4.5 and RCP8.5.

In general, the changes associated with the RCP8.5 scenario are greater than the corresponding changes associated with the RCP4.5 scenario, which is true for both mean and extreme wave heights, as shown in Figures 4 and 3.

Note that, even after the regional averaging and the 21 year moving averaging, the multidecadal variability of H_s is still discernible in the individual model projections, especially for the annual maximum H_s (see Figure 4, thin lines), although it disappears in the 20-model ensemble mean series (Figure 4, thick lines).

5. CMIP5 Versus CMIP3-Based Projections of Wave Height Changes

For the annual/seasonal mean H_s, the patterns of CMIP5-based projected changes (Figure 2, left) are similar to those shown in *Hemer et al.* [2013a, Figure 2], which used both dynamical and statistical wave modeling methods and are based on CMIP3 projections of SLP and surface winds for a different set of emissions

scenarios and a different set of global climate models. Despite these differences, both the CMIP3 and CMIP5-based wave projections show notable increases in annual/seasonal mean H_s in the SH high latitudes, with decreases in the SH midlatitudes and in the midlatitude North Atlantic (Figure 2, left). However, the CMIP5-based H_s projections (Figure 2) show much more extensive increases in the tropical South Pacific than the CMIP3-based H_s projections (especially in JFM); and in the tropical South Atlantic, the projected wave heights increase in CMIP5-based simulations but decrease in CMIP3-based simulations (compare *Hemer et al.* [2013a, Figure 2] with our Figure 2 (left)).

Since *Hemer et al.* [2013a] did not assess changes in extreme wave heights based on the CMIP3 simulations, a similar comparison between CMIP3 and CMIP5-based wave height projections cannot be made for projected changes in extreme wave heights.

6. Conclusions and Discussion

Our CMIP5-based statistical projections of changes in ocean wave heights show significant increases in ocean wave heights in the tropics (especially in the eastern tropical Pacific) and in the SH high latitudes (south of 45°S). These wave height increases are primarily driven by increases in SLP gradients in these regions, as shown in our supplementary analysis (see supporting information section S5 and the last paragraph below). The projected wave height increases (decreases) are accompanied by increased (decreased) variability of wave heights. In the North Pacific, the projected wave height changes show strong seasonality, with the eastern North Pacific being projected to have wave height increases in winter (the season of annual extreme wave heights) but decreases in summer.

Under the projected 2070–2099 climate condition of the rising high concentration pathway—the RCP8.5 scenario, the occurrence frequency of the present-day one in 10 year extreme wave heights is likely to double or triple in several coastal regions around the world, for example, the Chilean and Columbia's coasts, the Mexican Baja coast, the Vietnamese coast, the Tasmanian west coast, the Danish coast, the Gulf of Oman, the Gulf of Bengal, the South and East Asian coasts, and the Gulf of Mexico. The RCP8.5 and RCP4.5 scenarios share similar patterns of projected changes; but the changes associated with RCP4.5 are generally weaker than the corresponding changes associated with RCP8.5.

The impacts of changes in wave heights will also depend on changes in the local sea level. Global mean sea level rise was 0.19 (0.17 to 0.21) m over the period 1901–2010 and will likely be in the range of 0.45 to 0.82 m for the period 2081–2000 relative to the period 1986–2005 for the RCP8.5 scenario [*Alexander et al.*, 2013]. This will increase the impacts of the projected increases in wave heights. Since wave setup contributes to coastal sea level extremes and subsequent flooding, increased wave heights put the high coastal population at higher risk of inundation. Waves can cause overtopping of sea defences with consequent failure and damage to infrastructure or coastal erosion [*Hemer et al.*, 2012]. Thus, it is of critical importance for coastal and offshore infrastructure design to account for the combined effects of increased extreme wave heights on top of the rising mean sea level.

Changes in ocean wave heights are primarily driven by changes in surface winds, because ocean surface waves are generated by surface winds locally or remotely. This is confirmed by our supplementary analysis (see supporting information section S5), which shows that changes in annual mean wave heights share a similar pattern with changes in squared SLP spatial gradients (compare Figures 1a and S8b) and that changes in annual maximum wave heights share a similar pattern to changes in the annual maximum squared SLP spatial gradients (Figures 1b and S8c). Note that squared SLP spatial gradients represent geostrophic wind energy and were found to be a good predictor for ocean wave heights [*Wang et al.*, 2008, 2009; *Wang and Swail*, 2006a]. Analyzing a multimodel ensemble of CMIP3 simulations, *Wang et al.* [2008] found that changes in both geostrophic wind energy and ocean surface wave heights over the second half of the twentieth century are attributable to external forcing.

Acknowledgments

The authors are grateful to Rodney Chan for his help in downloading/preparing the large data sets, to Jean Bidlot of ECMWF for providing us with the ERA-Interim reanalysis data, to Nathan Gillett and Marjorie Shepherd for their helpful internal review of an earlier version of this manuscript, and to the CMIP5 modeling groups that provided the simulations used in this study.

The Editor thanks two anonymous reviewers for their assistance in evaluating this paper.

References

Alexander, L., et al. (2013), Summary for policymakers, in *Climate Change 2013: The Physical Science Basis. Working Group I Contribution to the IPCC 5th Assessment Report*, Stockholm, Sweden.

Box, G. E. P., and D. R. Cox (1964), An analysis of transformation (with discussion), *J. Roy. Stat. Soc. Ser. B*, *26*, 211–246.

Caires, S., A. Sterl, G. Komen, and V. Swail (2004a), The Web-based KNMI/ERA-40 global wave climatology atlas, *WMO Bulletin*, *53*, 142–146.

Caires, S., A. Sterl, J.-R. Bidlot, N. Graham, and V. Swail (2004b), Intercomparison of different wind-wave reanalyses, *J. Clim.*, *17*, 1893–1913.

Dee, D. P., et al. (2011), The ERA-Interim reanalysis: Configuration and performance of the data assimilation system, *Q. J. R. Meteorol. Soc.*, *137*(656), 553–597, doi:10.1002/gj.828.

Hemer, M. A., X. L. Wang, R. Weisse, and V. R. Swail (2012), Advancing wind-waves climate science, *Bull. Am. Meteor. Soc.*, *93*, 791–796, doi:10.1175/BAMS-D-11-00184.1.

Hemer, M. A., Y. Fan, N. Mori, A. Semedo, and X. L. Wang (2013a), Projected changes wave climate from a multi-model ensemble, *Nature Clim. Change*, *3*, 471–476, doi:10.1038/NCLIMATE1791.

Hemer, M. A., K. L. McInnes, and R. Ranasinghe (2013b), Projections of climate change-driven variations in the offshore wave climate off south eastern Australia, *Int. J. Climatol.*, *33*, 1615–1632, doi:10.1002/joc.3537.

Mori, N., T. Yasuda, H. Mase, T. Tom, and Y. Oku (2010), Projection of extreme wave climate change under global warming, *Hydrol. Res. Lett.*, *4*, 15–19, doi:10.3178/HRL.4.15.

Moss, R., et al. (2008), Towards new scenarios for analysis of emissions, climate change, impacts, and response strategies, *Technical Summary, The IPCC Expert Meeting Report*, Noordwijkerhout, Netherlands.

Nakicenovic, N., and R. Swart (eds.) (2000), *Special Report on Emissions Scenarios (SRES)*, 599 pp., Cambridge Univ. Press, Cambridge, U. K.

Taylor, K. E., R. J. Stouffer, and G. A. Meehl (2012), An overview of CMIP5 and the experiment design, *Bull. Am. Meteor. Soc.*, 485–498, doi:10.1175/BAMS-D-11-00094.1.

Uppala, S. M., et al. (2005), The ERA-40 re-analysis, *Q. J. R. Meteorol. Soc.*, *131*, 2961–3012.

Wang, X. L., and V. R. Swail (2006a), Climate change signal and uncertainty in projections of ocean wave heights, *Clim. Dyn.*, *26*, 109–126, doi:10.1007/s00382-005-0080-x.

Wang, X. L., and V. R. Swail (2006b), Historical and possible future changes of wave heights in northern hemisphere oceans, A chapter, in *Atmosphere Ocean Interactions,* vol. 2, edited by W. Perrie, pp. 240, Advances in Fluid Mechanics Series Vol 39, Wessex Institute of Technology Press, Southampton, U. K.

Wang, X. L., V. R. Swail, F. W. Zwiers, X. Zhang, and Y. Feng (2008), Detection of external influence on trends of atmospheric storminess and ocean wave heights, *Clim. Dyn.*, *32*, 189–203, doi:10.1007/s00382-008-0442-2.

Wang, X. L., V. R. Swail, and A. Cox (2009), Dynamical versus statistical downscaling methods for ocean wave heights, *Int. J. Climatol.*, *30*, 317–332, doi:10.1002/joc.1899.

Wang, X. L., Y. Feng, and V. R. Swail (2012), North Atlantic wave height trends as reconstructed from the twentieth century reanalysis, *Geophys. Res. Lett.*, *39*, L18705, doi:10.1029/2012GL053381.

Wang, X. L., B. Trewin, Y. Feng, and D. Jones (2013), Historical changes in Australian temperature extremes as inferred from extreme value distribution analysis, *Geophys. Res. Lett.*, *40*, 573–578, doi:10.1002/GRL.50132.

Young, I. R., S. Zieger, and A. V. Babanin (2011), Global trends in wind speed and wave height, *Science*, *332*, 451–455, doi:10.1126/science.1197219.

Young, I. R., J. Vinoth, S. Zieger, and A. V. Babanin (2012), Investigation of trends in extreme value wave height and wind speed, *J. Geophys. Res.*, *117*, C00J06, doi:10.1029/2011JC007753.